
Pretraining with Random Noise for Fast and Robust Learning without Weight Transport

Jeonghwan Cheon¹ Sang Wan Lee^{1,2,3} Se-Bum Paik¹

¹Department of Brain and Cognitive Sciences, ²Kim Jaechul Graduate School of AI,

³Center for Neuroscience-inspired Artificial Intelligence

Korea Advanced Institute of Science and Technology, Daejeon, Republic of Korea

{jeonghwan518, sangwan, sbpaik}@kaist.ac.kr

Abstract

The brain prepares for learning even before interacting with the environment, by refining and optimizing its structures through spontaneous neural activity that resembles random noise. However, the mechanism of such a process has yet to be thoroughly understood, and it is unclear whether this process can benefit the algorithm of machine learning. Here, we study this issue using a neural network with a feedback alignment algorithm, demonstrating that pretraining neural networks with random noise increases the learning efficiency as well as generalization abilities without weight transport. First, we found that random noise training modifies forward weights to match backward synaptic feedback, which is necessary for teaching errors by feedback alignment. As a result, a network with pre-aligned weights learns notably faster than a network without random noise training, even reaching a convergence speed comparable to that of a backpropagation algorithm. Sequential training with both random noise and data brings weights closer to synaptic feedback than training solely with data, enabling more precise credit assignment and faster learning. We also found that each readout probability approaches the chance level and that the effective dimensionality of weights decreases in a network pretrained with random noise. This pre-regularization allows the network to learn simple solutions of a low rank, reducing the generalization loss during subsequent training. This also enables the network robustly to generalize a novel, out-of-distribution dataset. Lastly, we confirmed that random noise pretraining reduces the amount of meta-loss, enhancing the network ability to adapt to various tasks. Overall, our results suggest that random noise training with feedback alignment offers a straightforward yet effective method of pretraining that facilitates quick and reliable learning without weight transport.

1 Introduction

The brain refines its network structure and synaptic connections even before birth, without exposure to sensory stimuli [1–26]. In the early developmental stages, the spontaneous neuronal activity that appears in various brain regions is considered to play a critical role during the development of neuronal circuits by pruning neural wirings and adjusting synaptic plasticity [27–31]. If this activity is disrupted during the developmental stages, the outcome can be long-lasting neuronal deficits. Computational studies suggest that such a refined network structure enables certain crucial functions of the brain, such as initializing function and efficient learning [32–35]. These experimental and theoretical studies commonly indicate that spontaneous, random neuronal activity plays a critical role in the development of the biological neural network before data are encountered by the network.

However, the detailed mechanism of how these prenatal processes contribute to learning after birth, i.e., with subsequent sensory stimuli, remains elusive.

At the synaptic level, learning can be defined as the process by which the brain adjusts the strength of synaptic connections between neurons to optimize the network for a specific task. The synaptic weights of each neuron can change to minimize the error between the expected and the actual output of a task, often referred to as the credit assignment problem [36]. However, in general, it is not well known how individual neurons modify these synaptic connections and thus achieve a network goal under a condition in which numerous neurons are linked in multiple layers. In other words, how neurons can estimate errors to modify their synaptic connections during learning remains unknown.

In machine learning, backpropagation algorithms have successfully addressed this issue – even in deep neural networks [37–39]. Backpropagation can provide feedback with regard to forward errors through the symmetric copying of forward weights via a backward process. During this process, a structural constraint, i.e., symmetric forward and backward weights, is necessary to assign proper error values to individual neurons [40, 41]. However, this process appears to be biologically implausible due to the weight transport problem [36, 42–44], in which individual neurons must somehow be aware of the exact synaptic connections of their downstream layers to update their weights, a state considered to be practically impossible in a biological brain.

An alternative algorithm, feedback alignment, achieves successful network training even without weight transport by employing fixed random feedback pathways [44]. Studies in relation to this show that a network can align its weights to synaptic feedback during data training, and this simple process enables error backpropagation. It has been shown that soft alignment between forward weights and synaptic feedback, which can be achieved during learning with massive amounts of data, is enough to back-propagate errors. This finding may provide a biologically plausible scenario in which the credit assignment problem can be resolved, yet there is an issue remaining — the process requires massive data learning to develop the structural constraint. This cannot be addressed even with currently known advanced learning rules [45, 46].

This situation is contradictory to the notion that the brain can learn even with very limited experience in the initial stages of life [47–50]. Thus, the question arises as to how early brains can estimate and assign errors for learning with limited experience. To address this issue, here we focus on the role of spontaneous activity at the prenatal stage in the brain, showing that training random noise, which mimics spontaneous random activity in prenatal brains, is a possible solution; random noise training aligns the forward weights to synaptic feedback, enabling precise credit assignment and fast learning. We also observed that random noise training can pre-regulate the weights and enable robust generalization. Our findings suggest that random noise training is a core mechanism of prenatal learning in biological brains and that it may provide a simple algorithm for the preconditioning of artificial neural networks for fast and robust learning without the weight transport process.

2 Preliminaries

Biological and artificial neural networks have different structures and functionalities, but they share certain factors in common, such that information is processed through multiple hierarchical layers of neurons with a nonlinear response function. In the current study, we consider a multi-layer feedforward neural network for pattern classification, $f_\theta : \mathbb{R}^m \rightarrow \mathbb{R}^d$, parameterized by $\theta = \{\mathbf{W}_l, \mathbf{b}_l\}_{l=0}^{L-1}$. It takes input $\mathbf{x} \in \mathbb{R}^m$ and outputs a vector $\mathbf{y} \in \mathbb{R}^d$ with L layers. Through a forward pass, the network computes a hidden layer output by propagating the input through the network layers, as follows:

$$\mathbf{o}_{l+1} = \mathbf{W}_l \mathbf{h}_l + \mathbf{b}_l, \quad \mathbf{h}_{l+1} = \phi(\mathbf{o}_{l+1}) \quad (1)$$

, where \mathbf{W}_l is the forward matrix, \mathbf{b}_l is the bias vector, and ϕ is the nonlinear activation function. In the first layer $l = 0$, $\mathbf{h}_l = \mathbf{x}$. We used a rectified linear unit (ReLU) activation function, $\phi(x) = \max(0, x)$. In the last layer $l = L - 1$, we used a softmax function, $\phi_y(x) = \text{softmax}(x) = \{e^{x_i} / \sum_{j=1}^d e^{x_j}\}_{i=1}^d$. Thus, the network outputs a probability distribution over d classes. After the forward pass, the amount of error is calculated by measuring the difference between the network output $f_\theta(\mathbf{x})$ and the target label \mathbf{y} . We used the cross-entropy loss [51], which is defined as follows:

$$\mathcal{L}(\theta) = -\frac{1}{N} \sum_{i=1}^N \sum_{j=1}^d y_{ij} \log f_{\theta}(\mathbf{x}_i)_j \quad (2)$$

, where N is the number of samples, d is the number of classes, and y_{ij} is the target label for the i -th sample and the j -th class. The purpose of learning is to minimize the error $\mathcal{L}(\theta)$. To achieve this, the network parameters θ are adjusted by assigning credit to the weights that contribute to the error, which is known as the credit assignment problem.

2.1 Backpropagation and weight transport problem

To solve the credit assignment problem, backpropagation [37] computes the gradient of errors with respect to the weights and uses it as a teaching signal to modulate the aforementioned parameters. The gradient is calculated by the chain rule, with propagation from the output layer to the input layer, as follows:

$$\delta_L = \frac{\partial \mathcal{L}}{\partial \mathbf{o}_L} = f_{\theta}(\mathbf{x}) - \mathbf{y}, \quad \delta_l = \frac{\partial \mathcal{L}}{\partial \mathbf{o}_l} = (\mathbf{W}_l^T \delta_{l+1}) \odot \phi'(\mathbf{o}_l) \quad (3)$$

, where δ_l is the error signal at layer l , ϕ' is the derivative of the activation function, and \odot denotes the element-wise product. The weight update rule is given by

$$\Delta \mathbf{W}_l = -\eta \delta_{l+1} \mathbf{h}_l^T \quad (4)$$

, where η is the learning rate. The backpropagation algorithm successfully solves the credit assignment problem, but it requires heavy computation to use the complete information of the synaptic weights of the next layer to update the current weights. Notably, backpropagation is considered as biologically implausible, because it is impossible, in the brain, to transmit the synaptic weights from the next layer to the current layer. This is known as the weight transport problem.

2.2 Feedback alignment

To address the weight transport problem, the idea of feedback alignment [44] was proposed as a biologically plausible alternative to backpropagation. In feedback alignment, the backward synaptic feedback is replaced with a random, fixed weight matrix \mathbf{B}_l in the feedback path, as follows:

$$\delta_l = \frac{\partial \mathcal{L}}{\partial \mathbf{o}_l} = (\mathbf{B}_l \delta_{l+1}) \odot \phi'(\mathbf{o}_l). \quad (5)$$

The only difference between backpropagation and feedback alignment is the replacement of the transpose of the forward matrix \mathbf{W}_l with the fixed random feedback matrix \mathbf{B}_l to calculate the error signal. The fact that the network can learn tasks from error teaching signals that are calculated from random feedback is explained by the observation that the network modifies the forward matrices \mathbf{W}_l to match the transpose of the feedback matrices \mathbf{B}_l roughly during training. This makes the error teaching signal (5) similar to backpropagation (3), thus enabling the network to learn the task.

3 Random noise training with feedback alignment

Algorithm 1 Random noise training

Input: Network $f_{\theta} : \mathbb{R}^m \rightarrow \mathbb{R}^d$, learning rate η , number of examples N_{examples} , batch size N_{batch}
Output: Trained network f_{θ}
for $i = 1$ to $N_{\text{examples}}/N_{\text{batch}}$ **do**
 \mathbf{x} from Gaussian distribution $\mathcal{N}(0, I)$, \mathbf{y} from discrete uniform distribution $\mathcal{U}(0, d-1)$
 Forward pass: $\hat{\mathbf{y}} = f_{\theta}(\mathbf{x})$
 Calculate loss: $\mathcal{L} = \text{cross_entropy}(\hat{\mathbf{y}}, \mathbf{y})$
 Backward pass: $\forall l, \mathbf{W}_l = \mathbf{W}_l - \eta \delta_l \mathbf{h}_l^T$
end for

During the developmental stage, spontaneous neural activity in the brain plays a critical role in shaping and refining neural circuits. Initially wired immature neural circuits undergo modifications of their connections through the processes of regulated cell formation, apoptosis, and synapse refinement through spontaneous neural activity [27–31]. These pre-sensory activities and development processes are universal across sensory modalities, such as the visual, auditory, and motor systems. We focus here on a few characteristics of spontaneous neural activity in the brain. Spontaneous neural activity is not correlated to external stimuli but can refine and optimize neural circuits, before interaction with the external world can take place.

Here, we propose a type of random training that is inspired by the spontaneous and prenatal neural activity in the brain to pretrain the neural network (Algorithm 1). In every batch, we sampled random noise inputs x from a Gaussian distribution $\mathcal{N}(0, I)$ and random labels y from a discrete uniform distribution $\mathcal{U}(0, N_{\text{readout}} - 1)$, without any correlation. The network f_{θ} was initialized with random weights and trained with the feedback alignment algorithm. In this study, we examined the effects of random noise training on the subsequent learning processes in model neural networks to understand the potential benefits of pretraining with random noise in biological brains and whether this strategy is applicable to machine learning algorithms.

4 Results

4.1 Weight alignment to synaptic feedback during random noise training

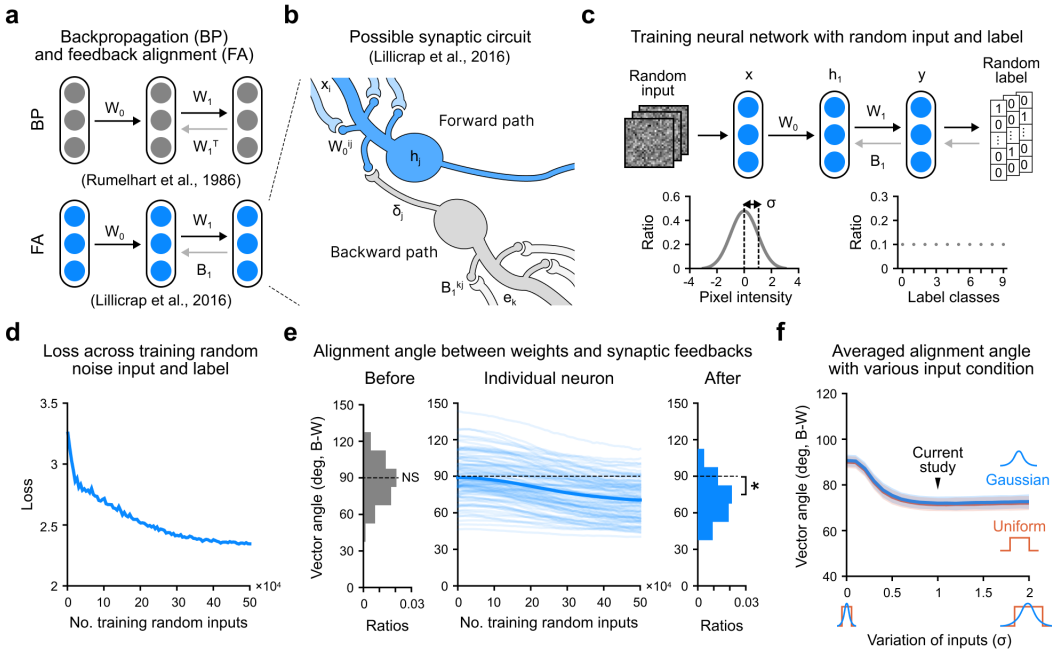


Figure 1: Weight alignment to randomly fixed synaptic feedback induced through random noise training. (a) Forward and backward pathways of backpropagation and feedback alignment. (b) Possible scenario of the feedback alignment algorithm in a biological synaptic circuit. (c) Schematic of random training, where the input x and label y are randomly sampled and paired in each iteration. (d) Cross-entropy loss during random training. (e) Alignment angle between forward weights and synaptic feedbacks in the last layer. (f) Alignment angle with various random input conditions.

To simulate a neural network initially wired by random weights and fixed random synaptic feedback, we adopted a network setting from the feedback alignment algorithm (Figure 1a) in which the weight transport problem can be avoided through the use of fixed random synaptic feedback. Thus, unlike backpropagation, this process is considered possibly to exist in biological neural networks with local synaptic connections (Figure 1b). We used a two-layer feedforward neural network with ReLU nonlinearity for classification, $f_{\theta} : \mathbb{R}^{784} \rightarrow \mathbb{R}^{10}$ with 100 neurons in the hidden layer. By means of

random noise training (Algorithm 1), we trained the neural network with random inputs sampled from a Gaussian distribution $\mathcal{N}(0, I)$, with labels also randomly sampled independently (Figure 1c).

We observed that the loss decreased noticeably during random training, even in the absence of meaningful data and even when \mathbf{x} and \mathbf{y} simply are randomly paired (Figure 1d). During the random training process, we focused on the alignment between the forward weights and the synaptic feedback. As described in the literature [44], the alignment of \mathbf{W}_l and \mathbf{B}_l , i.e., similarity between δ_{BP} and δ_{FA} , is crucial for calculating the error teaching signal precisely. To evaluate the alignment, we used cosine similarity, which is widely used for measuring the distance between two vectors.

Definition. Given the forward weights $\mathbf{W}_l \in \mathbb{R}^{m \times n}$ and backward weights $\mathbf{B}_l \in \mathbb{R}^{n \times n}$, we used the cosine angle as a measure of the alignment of individual neurons. We claim that \mathbf{W}_l and \mathbf{B}_l are aligned if $\mathbb{E}(\theta_i) = \mathbb{E}(\angle(\mathbf{W}_l^T)_i, (\mathbf{B}_l)_i)$ decreases asymptotically during training [44].

Notably, we found that the weights of neurons are aligned to the corresponding synaptic feedback weights during the random training process (Figure 1e). We also observed that the angle between the forward weights and synaptic feedback of individual neurons in the hidden layer decreased asymptotically during random training. In a randomly initialized network, the alignment angle appeared to be close to 90° , demonstrating that the backward error signal is randomly distributed (Figure 1e, left, alignment angle in an untrained network vs. 90° , $n = 100$, one-sample t-test, NS, $P = 0.492$). However, after random training, the alignment angle decreased significantly, implying that the backward teaching signal becomes valid to back-propagate errors (Figure 1d, right, alignment angle in an untrained network vs. a randomly trained network, $n = 100$, two-sample t-test, $*P < 0.001$). We confirmed that this is not simply due to input bias under a particular condition but is reproduced robustly with various input conditions (Figure 1f). These results suggest that neural networks can pre-learn how to back-propagate errors through random noise training.

4.2 Pretraining random noise enables fast learning during subsequent data training

Next, we compared networks with and without random training in terms of subsequent data training outcomes (Figure 2a). We trained the networks with the MNIST dataset [52], a widely used dataset for image classification benchmarking, finding that a randomly trained network can learn the data more quickly compared to a network without random training (Figure 2b). To quantify the speed of learning, we calculated the area under the curve (AUC) of the test accuracy and found that the convergence of the randomly trained network is significantly faster than that in the network without random training (Figure 2b, inset, untrained network vs. randomly trained network, $n_{Net} = 10$, t-test, $*P < 0.001$). Notably, the convergence speed of the randomly trained network appeared comparable to that of the network trained with backpropagation (Figure 2b, inset, randomly trained network vs. backpropagation, $n_{Net} = 10$, t-test, $*P < 0.001$). We also observed that the weight alignment gap between untrained and randomly trained networks is maintained during data training (Figure 2c). As a result, at the end of the data training step, the alignment angle of the randomly trained network was significantly smaller than that of the untrained network (Figure 2c, alignment angle in an untrained network vs. a randomly trained network, $n_{Net} = 10$, t-test, $*P < 0.001$). This result suggests that a combination of random pretraining and subsequent data training can enhance the weight alignment, which leads to more precise error teaching.

To understand the weight update dynamics by random and data training, we visualized the trajectory of weights in latent space as obtained by a principal component analysis (PCA) [53] (Figure 2d). We conducted PCA on the weights of the last layer (\mathbf{W}_1) for the random and data training conditions. First, we confirmed that in both random and data training, the weights become closer to synaptic feedback (Figure 2e, untrained vs. randomly trained network, $n_{Net} = 10$, t-test, $*P < 0.001$; untrained vs. data trained network, $n_{Net} = 10$, t-test, $*P < 0.001$; randomly trained network vs. data trained network, $n_{Net} = 10$, t-test, $*P < 0.001$). Notably, we observed that the updated trajectory of weights by random training and data training have different directions in the principal component space and that the effects of random training depend on the order of the random and data training (Figure 2f, g) — the enhancement of weight alignment was more significant when data training was performed after random training compared to when training is done in a reversed order. Particularly, when we trained the network with data first, subsequent random training could not move the weights (Figure 2g, data trained vs. data and random trained, $n_{Net} = 10$, t-test, NS, $P = 0.999$); thus, the weights did not become closer to synaptic feedback (Figure 2g, random trained vs. random and data trained, $n_{Net} = 10$, t-test, $*P < 0.001$). This result suggests that weight alignment by random noise

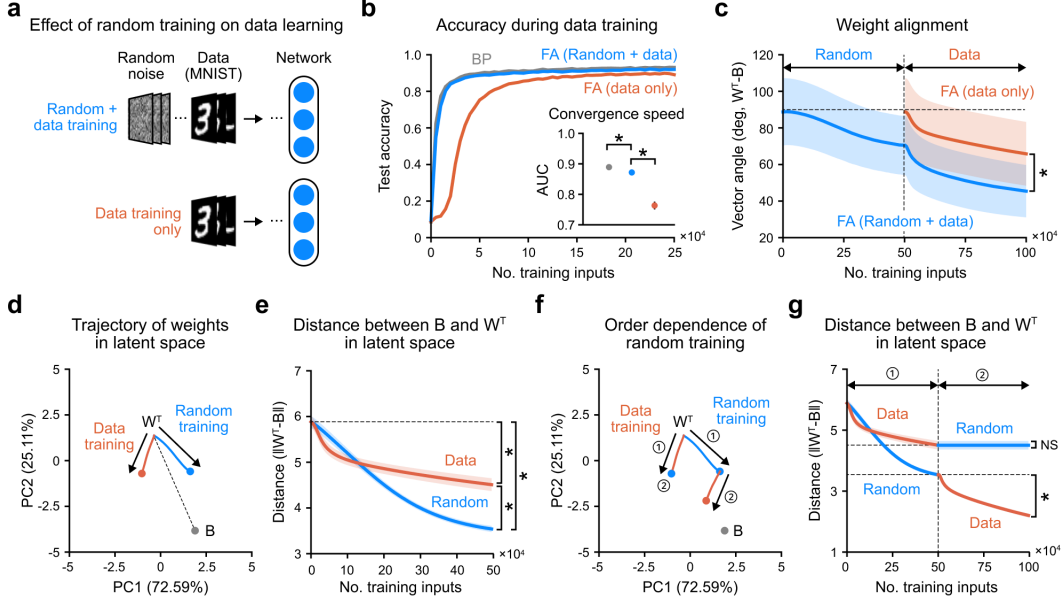


Figure 2: Effect of random noise training on subsequent data training. (a) Design of the MNIST classification task to investigate the effect of random training. (b) Test accuracy during the training process, where the inset demonstrates the convergence speed of each training method, calculated by the area under the curve (AUC) of the test accuracy. (c) Alignment angle between weights and synaptic feedback across random training and data training. (d) Trajectory of weights (W_1) toward synaptic feedback matrix (B_1) in latent space obtained by PCA (principal component analysis) for random and data training. (e) Distance between the weights (W_1) and the synaptic feedback matrix (B_1). (f) Order dependence of the trajectory of the weights (W_1). (g) Distance between the weights (W_1) and the synaptic feedback matrix (B_1) for different orders of random and data trainings.

pretraining cannot be replaced by data training and that it is crucial to perform random training prior to data training.

4.3 Pre-regularization by random noise training enables robust generalization

Next, we compared the difference between an untrained network and a randomly trained network in terms of their activation and weight (Figure 3a). First, we found that the readout probability of the untrained network is distributed over a wide range (Figure 3b, left, readout probability vs. chance level, $n = 10,000$, one-sample t-test, $*P < 0.001$), whereas that of the randomly trained network is well regularized, close to the chance level (Figure 3b, right, readout probability vs. chance level, $n = 10,000$, one-sample t-test, NS, $P = 0.371$). We also observed that the singular value spectrum of forward weights changes significantly by random training (Figure 3c) such that a small portion of singular values become dominant in the randomly trained network. To measure the effective dimensionality of the weights quantitatively, we used the effective rank of the weights.

Definition. Given a matrix $A \in \mathbb{R}^{m \times n}$ is decomposed into $A = U\Sigma V^T$ by singular value decomposition (SVD), the singular values are $\{\sigma_i\}_i^{min(m,n)}$ sorted in a descending order. The effective rank ρ is defined as the Shannon entropy of the normalized singular values, $\rho = -\sum_i \bar{\sigma}_i \log \bar{\sigma}_i$, where $\bar{\sigma}_i = \sigma_i / \sum_i \sigma_i$. Without loss of generality, we used the effective rank as the exponential of ρ [54].

We observed that the effective rank of forward weights decreased significantly during random training (Figure 3d), implying that random training regularizes the weights initially and predisposes the network to learn simple solutions of a low rank. Given the notion that low-rank solutions show better generalization performance outcomes, we hypothesized that this pre-regularization by random training enables robust generalization during subsequent data training by inducing low-rank solutions.

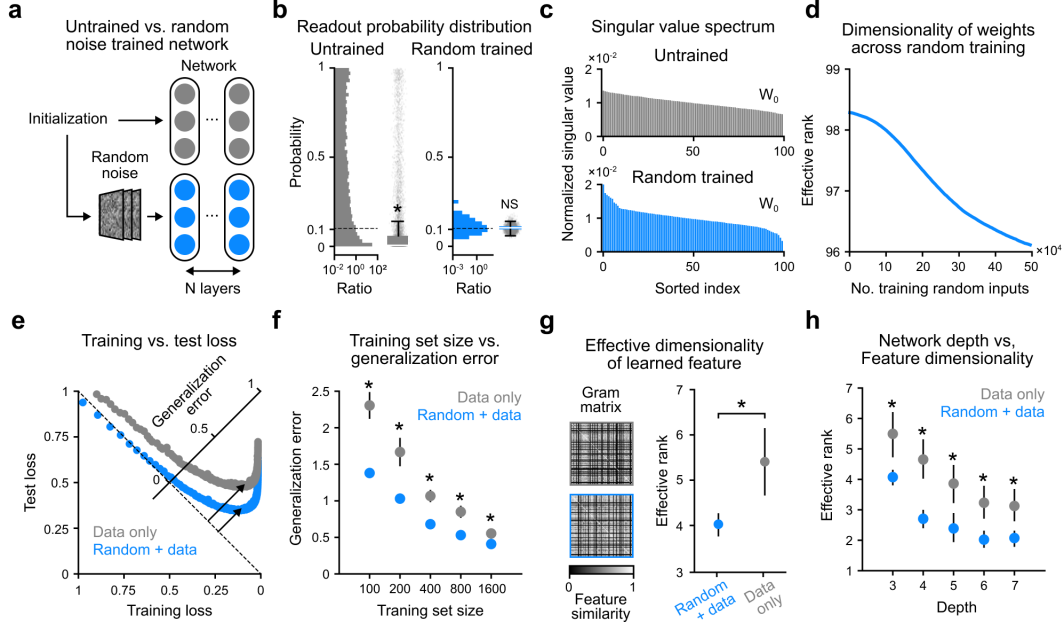


Figure 3: Pre-regularization by random noise training enhances generalization (a) Untrained network and pre-regularized network through random noise training. (b) Distribution of the readout probability. (c) Singular value spectrum of the forward weights. (d) Effective rank of forward weights during random noise training. (e) Generalization error gap between the training error and test error (training set size: 1600, network depth: 3). (f) Generalization error for various training set sizes (network depth: 3). (g) Effective dimensionality of the Gram matrix, the cosine similarity of feature vectors across neurons (training set size: 1600, network depth: 3). (h) Effective dimensionality of the Gram matrix for various network depths (training set size: 1600).

To test the generalization ability of the network, we measured the gap between the training error and the test error during subsequent data training. We observed that the generalization error was noticeably lower in a randomly trained network compared to an untrained network (Figure 3e) and that this tendency was maintained with variations of the training set size (Figure 3f, random and data trained vs. data trained, $n_{\text{Net}} = 10$, t-test, $*P < 0.001$). This result suggests that pre-regularization by random training can enable robust generalization during subsequent data training.

Next, we compared the representation of learned features in an untrained network and a randomly trained network. We used the Gram matrix, defined as the cosine similarity of feature vectors across neurons. Notably, we found that the effective rank of the Gram matrix was significantly lower in a randomly trained network compared to an untrained network after subsequent data training (Figure 3g, random and data trained vs. data trained, $n_{\text{Net}} = 10$, t-test, $*P < 0.001$) and that this tendency was maintained regardless of the network depth (Figure 3h, random and data trained vs. data trained, $n_{\text{Net}} = 10$, t-test, $*P < 0.001$). This finding suggests that pre-regularization by random training can enable networks to learn simpler solutions, leading to better generalization performance during subsequent data training.

We also tested the generalization performance of the networks for “out-of-distribution” tasks by training the network with the MNIST dataset and testing it with various out-of-distribution tasks (Figure 4a). First, we generated a MNIST dataset of translated, rotated, and scaled images and then used these images as out-of-distribution tasks (Figure 4b, left). We observed that a randomly trained network showed significantly higher test accuracy on out-of-distribution tasks than an untrained network (Figure 4b, right, random and data trained vs. data trained, $n_{\text{Net}} = 10$, t-test, $*P < 0.001$). We also observed that the randomly trained network showed higher test accuracy on the USPS dataset, which is a widely used benchmark dataset for out-of-distribution tasks (Figure 4c, random and data trained vs. data trained, $n_{\text{Net}} = 10$, t-test, $*P < 0.001$). This result suggests that pre-regularization by random training enables robust out-of-distribution generalization during subsequent data training.

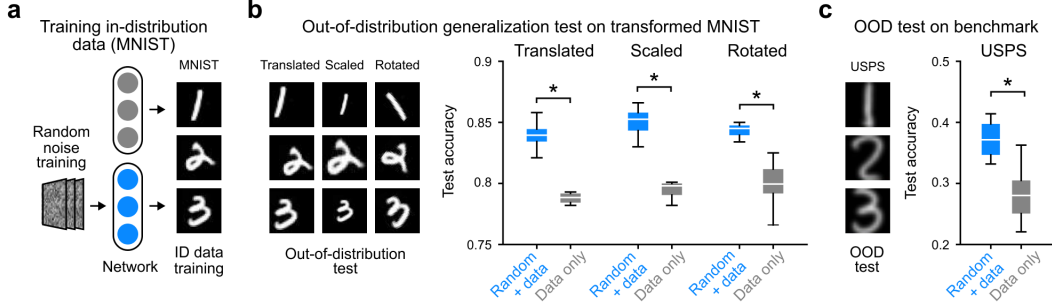


Figure 4: Robust generalization of “out-of-distribution“ tasks in randomly trained networks. (a) Training in-distribution data (MNIST) in untrained and randomly trained networks. (b) Out-of-distribution generalization tests on transformed MNIST. (c) Out-of-distribution generalization tests on USPS dataset.

4.4 Task-agnostic fast learning for various tasks by a network pretrained with random noise

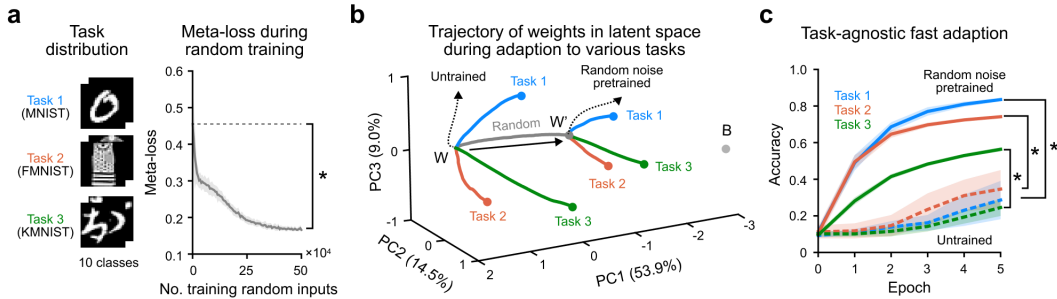


Figure 5: Task-agnostic fast learning for various tasks in randomly trained networks. (a) Three tasks used to test the task-agnostic property of random training, showing the meta-loss during the random training process. The meta-loss is calculated from the sum of the losses measured during adaption to each task. (b) Trajectory of weights in the latent space during adaptation to each task of an untrained network and a randomly trained network. (c) Adaption to each task of an untrained network and a randomly trained network.

Lastly, we examined whether random training is task-agnostic. We compared the task adaption capacity of an untrained network and a randomly trained network on three tasks: (1) MNIST classification [52], (2) Fashion-MNIST [55], (3) Kuzushiji-MNIST [56] (Figure 5a, left). To measure the ability of fast adaption to various tasks quantitatively, we computed the meta-loss, as suggested in a previous study of meta-learning.

Definition. Given the task distribution $\mathcal{T} \in \{\mathcal{T}_i\}_i^n$, the meta-loss of network f_θ is defined as $\mathcal{L}_{\text{meta}}(\theta) = \sum_{\mathcal{T}_i \in \mathcal{T}} \mathcal{L}_{\mathcal{T}_i}(\theta'_i)$, where $\mathcal{L}_{\mathcal{T}_i}(\theta'_i)$ denotes the loss of the task \mathcal{T}_i and θ'_i is the adapted parameter for \mathcal{T}_i [57].

We observed that the meta-loss decreased gradually during the random training process (Figure 5a, right). Considering that the training was solely performed with random inputs and labels on the three tasks to measure the meta-loss, this result suggests that networks can learn how to adapt to various tasks without any task-specific data. Next, we trained the untrained networks and random noise trained networks on each task separately. We conducted principal component analysis (PCA) on the weights of the last layer (\mathbf{W}_2) to visualize the trajectory of weights in latent space during the adaption to each task. We observed that the trajectory of weights during random noise training moves closer to synaptic feedback (\mathbf{B}_2), which makes the adaption to each task more efficient (Figure 5b). This suggests that random training is task-agnostic but provides efficient and fast learning in subsequent learning (Figure 5b). Lastly, we compared the adaption to each task in an untrained network and a

randomly trained network. We observed that the randomly trained network showed remarkably fast adaption to each task compared to the untrained network (Figure 5c, random and data trained vs. data trained, $n_{\text{Net}} = 10$, t-test, $*P < 0.001$). These results highlight the task-agnostic property of random training, which enables networks quickly to adapt to various tasks.

5 Discussion

We showed that random noise training enables neural networks to learn quickly and robustly without weight transport. This finding bridges the gap between a biologically plausible learning mechanism and the conventional backpropagation algorithm, as symmetry of forward and backward weights can easily be achieved by random noise training. Moreover, the results here provide new insight into the advantage of random training as a means of pre-regularization of a network for robust generalization.

Insights into developmental neuroscience. Unlike artificial neural networks, the brain is ready to learn before encountering data. In the early developmental stage before eye-opening, spontaneous random activity emerges in the brain, which is considered essential for a normal development of early circuits. However, the functional advantage of learning from random noise before external sensory inputs remains unclear. Our study provides a plausible scenario that the brain utilizes spontaneous random activity to pre-align the synaptic weights for error learning and pre-regularization of synaptic connections for robust generalization. Specifically, we showed that random training reduces the effective dimensionality of the weights, which can be considered as a form of pruning, as previous neuroscience studies reported that the brain’s synaptic connections are pruned substantially during development, particularly dependent on spontaneous activity [27–31]. Despite the fact that the present study is based on model neural networks, the results here are consistent with a range of experimental findings in developmental neuroscience.

Error-backpropagation without weight transport. Understanding how the brain can efficiently learn is a collective goal among neuroscience and artificial intelligence researchers. Early works by neuroscientists have suggested several naive learning rules, such as Hebbian learning [58] and spike-timing-dependent plasticity (STDP) [59–61]. Although these rules have been experimentally observed and are thus biologically plausible, they are not sufficient to explain the brain’s remarkable learning ability thoroughly [62, 63]. On the other hand, while the backpropagation algorithms used in artificial neural networks have shown impressive learning capabilities, they are considered biologically implausible due to the weight transport problem [36]. Our results provide a new perspective on this issue, bridging the gap between these training rules. We showed that symmetry among forward and backward weights, which is necessary to back-propagate errors, can be readily developed by learning random noise, similar to that during the brain’s prenatal stage. Our findings suggest a probable scenario for significantly narrowing the performance gap between previously suggested biologically plausible learning rules and backpropagation.

Pre-regularization for robust generalization. We suggest a task- and model-agnostic pretraining strategy that involves simply training the network with random noise. Notably, our results here show that random noise training can enhance the learning efficiency and generalization ability of the network, for which various tricks and techniques have been proposed to improve. We found that pretraining on random noise reduces the effective dimensionality of the weights, which leads to the learning of low-rank solutions for tasks. Previous studies on generalization have shown that the low-rank bias of neural networks is crucial for their generalization ability, as we confirmed here [64–68]. Also, our results showed that the complexity of the representation is significantly reduced in a network pretrained with random noise, which might be a type of information bottleneck [69–73]. Also, the refinement of readout activity to the chance level suggests that random noise training can transform the loss function of the network to a smoother and more sensitive form for learning [74–76]. It is also important to note that the simple strategy of random noise training can have various effects on the network’s learning dynamics that previous machine learning techniques have aimed to achieve. This may be a possible strategy employed by the brain to achieve notable generalization ability. At the same time, it suggests a new form of pretraining strategy for artificial neural networks.

6 Limitations and Broader Impacts

Limitations. Although our study provides a new perspective on the role of spontaneous random activity in the brain, there are several limitations to consider. We used a fully connected feedforward neural network. It shares some similarities with biological neural networks, but they are distinct in terms of structure and function. Also, we used a feedback alignment algorithm to train the networks. As it does not utilize weight transport, further experimental studies are needed to confirm our results in actual biological systems.

Broader impacts. Feedback alignment algorithm and its advanced modifications without weight transport are motivated by the need to suggest a learning method that is compatible with deep neural networks with biological plausibility. It can be useful particularly when implemented in physical circuits, as nowadays deep learning without weight transport is utilized in neuromorphic chip engineering. Given that backpropagation requires dynamic access to memory due to weight transport, it is not free from the issue of energy inefficiency. Our results are not solely limited to demonstrating the role of biological prenatal learning but can also be extended for more practical purposes; for instance, it is a promising strategy for the preconditioning of neuromorphic chips.

Acknowledgements

This work was supported by the National Research Foundation of Korea (NRF-2022R1A2C3008991 to S.P.) and by the Singularity Professor Research Project of KAIST (to S.P.).

References

- [1] Mar Anfbal-Martínez, Lorenzo Puche-Aroca, Gabriele Pumo, Dorien Vandael, M Pilar Madrigal, Luis Miguel Rodríguez-Malmierca, Miguel Valdeolmillos, Francisco Jose Martini, Filippo M Rijli, and Guillermina López-Bendito. Prenatal tuning of thalamic spontaneous activity patterns regulates somatosensory map resolution. *bioRxiv*, pages 2024–03, 2024.
- [2] Mark V Albert, Adam Schnabel, and David J Field. Innate visual learning through spontaneous activity patterns. *PLoS Computational Biology*, 4(8):e1000137, 2008.
- [3] Lilach Avitan, Zac Pujic, Jan Mölter, Matthew Van De Poll, Biao Sun, Haotian Teng, Rumelo Amor, Ethan K Scott, and Geoffrey J Goodhill. Spontaneous activity in the zebrafish tectum reorganizes over development and is influenced by visual experience. *Current Biology*, 27(16):2407–2419, 2017.
- [4] Heiko J Luhmann, Anne Sinning, Jenq-Wei Yang, Vicente Reyes-Puerta, Maik C Stüttgen, Sergei Kirischuk, and Werner Kilb. Spontaneous neuronal activity in developing neocortical networks: from single cells to large-scale interactions. *Frontiers in neural circuits*, 10:40, 2016.
- [5] Richard H Masland. Maturation of function in the developing rabbit retina. *Journal of Comparative Neurology*, 175(3):275–286, 1977.
- [6] Lucia Galli and Lamberto Maffei. Spontaneous impulse activity of rat retinal ganglion cells in prenatal life. *Science*, 242(4875):90–91, 1988.
- [7] James B Ackman, Timothy J Burbridge, and Michael C Crair. Retinal waves coordinate patterned activity throughout the developing visual system. *Nature*, 490(7419):219–225, 2012.
- [8] Jing Shen and Matthew T Colonnese. Development of activity in the mouse visual cortex. *Journal of Neuroscience*, 36(48):12259–12275, 2016.
- [9] Andrew Thompson, Alexandra Gribizis, Chinfei Chen, and Michael C Crair. Activity-dependent development of visual receptive fields. *Current opinion in neurobiology*, 42:136–143, 2017.
- [10] James B Ackman and Michael C Crair. Role of emergent neural activity in visual map development. *Current opinion in neurobiology*, 24:166–175, 2014.
- [11] Wai T Wong, Joshua R Sanes, and Rachel OL Wong. Developmentally regulated spontaneous activity in the embryonic chick retina. *Journal of Neuroscience*, 18(21):8839–8852, 1998.
- [12] Calvin J Kersbergen, Travis A Babola, Jason Rock, and Dwight E Bergles. Developmental spontaneous activity promotes formation of sensory domains, frequency tuning and proper gain in central auditory circuits. *Cell reports*, 41(7), 2022.

- [13] M Geal-Dor, S Freeman, G Li, and H Sohmer. Development of hearing in neonatal rats: air and bone conducted abr thresholds. *Hearing research*, 69(1-2):236–242, 1993.
- [14] Xiangying Meng, Krystyna Solarana, Zac Bowen, Ji Liu, Daniel A Nagode, Aminah Sheikh, Daniel E Winkowski, Joseph PY Kao, and Patrick O Kanold. Transient subgranular hyperconnectivity to I2/3 and enhanced pairwise correlations during the critical period in the mouse auditory cortex. *Cerebral Cortex*, 30(3):1914–1930, 2020.
- [15] Helen J Kennedy. New developments in understanding the mechanisms and function of spontaneous electrical activity in the developing mammalian auditory system. *Journal of the Association for Research in Otolaryngology*, 13:437–445, 2012.
- [16] Alexandra H Leighton and Christian Lohmann. The wiring of developing sensory circuits—from patterned spontaneous activity to synaptic plasticity mechanisms. *Frontiers in neural circuits*, 10:71, 2016.
- [17] Han Chin Wang and Dwight E Bergles. Spontaneous activity in the developing auditory system. *Cell and tissue research*, 361:65–75, 2015.
- [18] Mandy Sonntag, Bernhard Englitz, Cornelia Kopp-Scheinflug, and Rudolf Rübsamen. Early postnatal development of spontaneous and acoustically evoked discharge activity of principal cells of the medial nucleus of the trapezoid body: an in vivo study in mice. *Journal of Neuroscience*, 29(30):9510–9520, 2009.
- [19] Scott R Robinson, Mark S Blumberg, Maura S Lane, and Lisa S Kreber. Spontaneous motor activity in fetal and infant rats is organized into discrete multilimb bouts. *Behavioral neuroscience*, 114(2):328, 2000.
- [20] Viktor Hamburger and CH Narayanan. Effects of the deafferentation of the trigeminal area on the motility of the chick embryo. *Journal of Experimental Zoology*, 170(4):411–426, 1969.
- [21] Viktor Hamburger, Eleanor Wenger, and Ronald Oppenheim. Motility in the chick embryo in the absence of sensory input. *Journal of Experimental Zoology*, 162(2):133–159, 1966.
- [22] RR Provine, SC Sharma, TT Sandel, and V Hamburger. Electrical activity in the spinal cord of the chick embryo, in situ. *Proceedings of the National Academy of Sciences*, 65(3):508–515, 1970.
- [23] Ana R Inácio, Azat Nasretidinov, Julia Lebedeva, and Roustem Khazipov. Sensory feedback synchronizes motor and sensory neuronal networks in the neonatal rat spinal cord. *Nature communications*, 7(1):13060, 2016.
- [24] Takuji Iwasato and Reha S Erzurumlu. Development of tactile sensory circuits in the CNS. *Current opinion in neurobiology*, 53:66–75, 2018.
- [25] Noelia Antón-Bolaños, Alejandro Sempere-Ferrández, Teresa Guillamón-Vivancos, Francisco J Martini, Leticia Pérez-Saiz, Henrik Gezelius, Anton Filipchuk, Miguel Valdeolmillos, and Guillermina López-Bendito. Prenatal activity from thalamic neurons governs the emergence of functional cortical maps in mice. *Science*, 364(6444):987–990, 2019.
- [26] Hidenobu Mizuno, Koji Ikezoe, Shingo Nakazawa, Takuya Sato, Kazuo Kitamura, and Takuji Iwasato. Patchwork-type spontaneous activity in neonatal barrel cortex layer 4 transmitted via thalamocortical projections. *Cell reports*, 22(1):123–135, 2018.
- [27] Francisco J Martini, Teresa Guillamón-Vivancos, Verónica Moreno-Juan, Miguel Valdeolmillos, and Guillermina López-Bendito. Spontaneous activity in developing thalamic and cortical sensory networks. *Neuron*, 109(16):2519–2534, 2021.
- [28] Oriane Blanquie, Jenq-Wei Yang, Werner Kilb, Salim Sharopov, Anne Sinning, and Heiko J Luhmann. Electrical activity controls area-specific expression of neuronal apoptosis in the mouse developing cerebral cortex. *Elife*, 6:e27696, 2017.
- [29] Larry C Katz and Carla J Shatz. Synaptic activity and the construction of cortical circuits. *Science*, 274(5290):1133–1138, 1996.
- [30] Werner Kilb, Sergei Kirischuk, and Heiko J Luhmann. Electrical activity patterns and the functional maturation of the neocortex. *European Journal of Neuroscience*, 34(10):1677–1686, 2011.
- [31] Nobuhiko Yamamoto and Guillermina López-Bendito. Shaping brain connections through spontaneous neural activity. *European Journal of Neuroscience*, 35(10):1595–1604, 2012.

- [32] Gwangsu Kim, Jaeson Jang, Seungdae Baek, Min Song, and Se-Bum Paik. Visual number sense in untrained deep neural networks. *Science advances*, 7(1):eabd6127, 2021.
- [33] Seungdae Baek, Min Song, Jaeson Jang, Gwangsu Kim, and Se-Bum Paik. Face detection in untrained deep neural networks. *Nature communications*, 12(1):7328, 2021.
- [34] Jeonghwan Cheon, Seungdae Baek, and Se-Bum Paik. Invariance of object detection in untrained deep neural networks. *Frontiers in Computational Neuroscience*, 16:1030707, 2022.
- [35] Hyeonsu Lee, Wochul Choi, Dongil Lee, and Se-Bum Paik. Comparison of visual quantities in untrained neural networks. *Cell Reports*, 42(8), 2023.
- [36] Timothy P Lillicrap, Adam Santoro, Luke Marris, Colin J Akerman, and Geoffrey Hinton. Backpropagation and the brain. *Nature Reviews Neuroscience*, 21(6):335–346, 2020.
- [37] David E. Rumelhart, Geoffrey E. Hinton, and Ronald J. Williams. Learning representations by back-propagating errors. *Nature*, 323:533–536, 10 1986.
- [38] Alex Krizhevsky, Ilya Sutskever, and Geoffrey E Hinton. Imagenet classification with deep convolutional neural networks. *Advances in neural information processing systems*, 25, 2012.
- [39] Yann LeCun, Yoshua Bengio, and Geoffrey Hinton. Deep learning. *nature*, 521(7553):436–444, 2015.
- [40] Andrew M Saxe, James L McClelland, and Surya Ganguli. Exact solutions to the nonlinear dynamics of learning in deep linear neural networks. *arXiv preprint arXiv:1312.6120*, 2013.
- [41] Konrad P Körding and Peter König. Supervised and unsupervised learning with two sites of synaptic integration. *Journal of computational neuroscience*, 11:207–215, 2001.
- [42] Stephen Grossberg. Competitive learning: From interactive activation to adaptive resonance. *Cognitive science*, 11(1):23–63, 1987.
- [43] Francis Crick. The recent excitement about neural networks. *Nature*, 337(6203):129–132, 1989.
- [44] Timothy P Lillicrap, Daniel Cownden, Douglas B Tweed, and Colin J Akerman. Random synaptic feedback weights support error backpropagation for deep learning. *Nature communications*, 7(1):13276, 2016.
- [45] Mohamed Akrouf, Collin Wilson, Peter Humphreys, Timothy Lillicrap, and Douglas B Tweed. Deep learning without weight transport. *Advances in neural information processing systems*, 32, 2019.
- [46] Arild Nøkland. Direct feedback alignment provides learning in deep neural networks. *Advances in neural information processing systems*, 29, 2016.
- [47] Tiffany M Field, Debra Cohen, Robert Garcia, and Reena Greenberg. Mother-stranger face discrimination by the newborn. *Infant Behavior and development*, 7(1):19–25, 1984.
- [48] IWR Bushneil, F Sai, and Jim T Mullin. Neonatal recognition of the mother’s face. *British journal of developmental psychology*, 7(1):3–15, 1989.
- [49] Olivier Pascalis, Scania de Schonen, John Morton, Christine Deruelle, and Marie Fabre-Grenet. Mother’s face recognition by neonates: A replication and an extension. *Infant behavior and development*, 18(1):79–85, 1995.
- [50] Traer Scott. *Wild Babies: Photographs of Baby Animals from Giraffes to Hummingbirds*. Chronicle Books, 2016.
- [51] Irving John Good. Rational decisions. *Journal of the Royal Statistical Society: Series B (Methodological)*, 14(1):107–114, 1952.
- [52] Li Deng. The mnist database of handwritten digit images for machine learning research. *IEEE signal processing magazine*, 29(6):141–142, 2012.
- [53] Svante Wold, Kim Esbensen, and Paul Geladi. Principal component analysis. *Chemometrics and Intelligent Laboratory Systems*, 2:37–52, 8 1987.
- [54] Olivier Roy and Martin Vetterli. The effective rank: A measure of effective dimensionality. In *2007 15th European signal processing conference*, pages 606–610. IEEE, 2007.
- [55] Han Xiao, Kashif Rasul, and Roland Vollgraf. Fashion-mnist: a novel image dataset for benchmarking machine learning algorithms. *arXiv preprint arXiv:1708.07747*, 2017.

- [56] Tarin Clanuwat, Mikel Bober-Irizar, Asanobu Kitamoto, Alex Lamb, Kazuaki Yamamoto, and David Ha. Deep learning for classical japanese literature. *arXiv preprint arXiv:1812.01718*, 2018.
- [57] Chelsea Finn, Pieter Abbeel, and Sergey Levine. Model-agnostic meta-learning for fast adaptation of deep networks. In *International conference on machine learning*, pages 1126–1135. PMLR, 2017.
- [58] Donald Olding Hebb. *The organization of behavior: A neuropsychological theory*. Psychology press, 1949.
- [59] Robert C Froemke and Yang Dan. Spike-timing-dependent synaptic modification induced by natural spike trains. *Nature*, 416(6879):433–438, 2002.
- [60] Yang Dan and Mu-ming Poo. Spike timing-dependent plasticity of neural circuits. *Neuron*, 44(1):23–30, 2004.
- [61] Natalia Caporale and Yang Dan. Spike timing-dependent plasticity: a hebbian learning rule. *Annu. Rev. Neurosci.*, 31:25–46, 2008.
- [62] H Sebastian Seung. Learning in spiking neural networks by reinforcement of stochastic synaptic transmission. *Neuron*, 40(6):1063–1073, 2003.
- [63] Yiting Dong, Dongcheng Zhao, Yang Li, and Yi Zeng. An unsupervised stdp-based spiking neural network inspired by biologically plausible learning rules and connections. *Neural Networks*, 165:799–808, 2023.
- [64] Sanjeev Arora, Nadav Cohen, Wei Hu, and Yuping Luo. Implicit regularization in deep matrix factorization. *Advances in Neural Information Processing Systems*, 32, 2019.
- [65] Minyoung Huh, Hossein Mobahi, Richard Zhang, Brian Cheung, Pulkit Agrawal, and Phillip Isola. The low-rank simplicity bias in deep networks. *arXiv preprint arXiv:2103.10427*, 2021.
- [66] Aristide Baratin, Thomas George, César Laurent, R Devon Hjelm, Guillaume Lajoie, Pascal Vincent, and Simon Lacoste-Julien. Implicit regularization via neural feature alignment. In *International Conference on Artificial Intelligence and Statistics*, pages 2269–2277. PMLR, 2021.
- [67] Dan Zhao. Combining explicit and implicit regularization for efficient learning in deep networks. *Advances in Neural Information Processing Systems*, 35:3024–3038, 2022.
- [68] Parth Natekar and Manik Sharma. Representation based complexity measures for predicting generalization in deep learning. *arXiv preprint arXiv:2012.02775*, 2020.
- [69] Naftali Tishby, Fernando C Pereira, and William Bialek. The information bottleneck method. *arXiv preprint physics/0004057*, 2000.
- [70] Naftali Tishby and Noga Zaslavsky. Deep learning and the information bottleneck principle. In *2015 IEEE information theory workshop (itw)*, pages 1–5. IEEE, 2015.
- [71] Kenji Kawaguchi, Zhun Deng, Xu Ji, and Jiaoyang Huang. How does information bottleneck help deep learning? In *International Conference on Machine Learning*, pages 16049–16096. PMLR, 2023.
- [72] Ravid Shwartz-Ziv and Naftali Tishby. Opening the black box of deep neural networks via information. *arXiv preprint arXiv:1703.00810*, 2017.
- [73] Andrew M Saxe, Yamini Bansal, Joel Dapello, Madhu Advani, Artemy Kolchinsky, Brendan D Tracey, and David D Cox. On the information bottleneck theory of deep learning. *Journal of Statistical Mechanics: Theory and Experiment*, 2019(12):124020, 2019.
- [74] Hao Li, Zheng Xu, Gavin Taylor, Christoph Studer, and Tom Goldstein. Visualizing the loss landscape of neural nets. *Advances in neural information processing systems*, 31, 2018.
- [75] Ping-yeh Chiang, Renkun Ni, David Yu Miller, Arpit Bansal, Jonas Geiping, Micah Goldblum, and Tom Goldstein. Loss landscapes are all you need: Neural network generalization can be explained without the implicit bias of gradient descent. In *The Eleventh International Conference on Learning Representations*, 2022.
- [76] Ali Akbari, Muhammad Awais, Manijeh Bashar, and Josef Kittler. How does loss function affect generalization performance of deep learning? application to human age estimation. In *International Conference on Machine Learning*, pages 141–151. PMLR, 2021.
- [77] Alex Krizhevsky, Geoffrey Hinton, et al. Learning multiple layers of features from tiny images. 2009.
- [78] Jonathan J. Hull. A database for handwritten text recognition research. *IEEE Transactions on pattern analysis and machine intelligence*, 16(5):550–554, 1994.

A Experimental details and additional results for section 4.1

A.1 Network architecture and training details

Table A.1: Parameters and settings used in the experiment.

| Network architecture | |
|-----------------------|-----------------|
| Name | Setting |
| Dimensions | [784, 100, 10] |
| Activation function | ReLU |
| Random noise training | |
| Name | Setting |
| Number of examples | 5×10^5 |
| Batch size | 64 |
| Learning rate | 0.0001 |
| Optimizer | Adam |

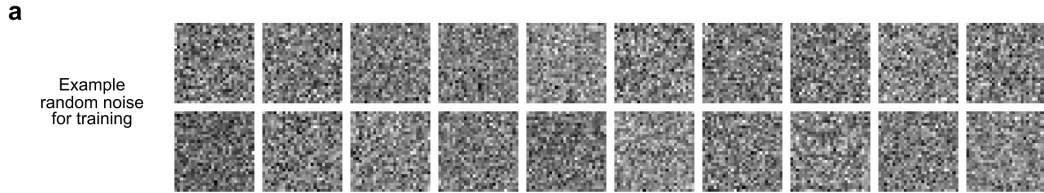


Figure A.1: Samples of random noise used in the pretraining process. Each pixel value is randomly drawn from a zero-centered Gaussian distribution with a standard deviation of 1. The corresponding label is also randomly assigned from a discrete uniform distribution [0,9].

B Experimental details and additional results for section 4.2

B.1 Network architecture and training details

Table B.1: Parameters and settings used in the experiment.

| Network architecture | |
|-------------------------|------------------|
| Name | Setting |
| Dimensions | $[784, 100, 10]$ |
| Activation function | ReLU |
| MNIST data training | |
| Name | Setting |
| Number of training data | 5×10^3 |
| Number of test data | 5×10^3 |
| Epochs | 100 |
| Batch size | 64 |
| Learning rate | 0.0001 |
| Optimizer | Adam |



Figure B.1: Samples from the MNIST data [52] used in the subsequent data training process. The dataset contains images of handwritten digits with ten classes.

B.2 Training results

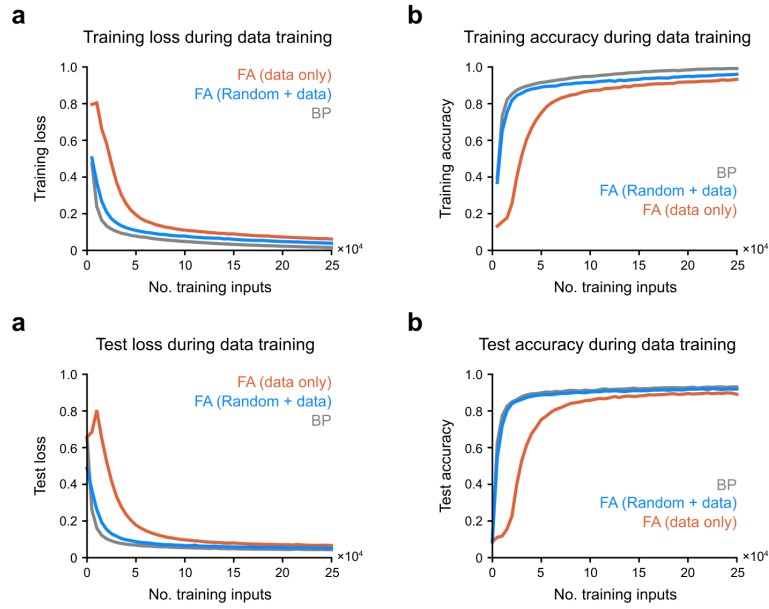


Figure B.2: Loss and accuracy outcomes of the network under various training conditions. (a) Training loss. (b) Test loss. (c) Training accuracy. (d) Test accuracy. Blue and orange lines denote the network trained with feedback alignment with and without random noise training, respectively. Gray lines represent the network trained with backpropagation.

B.3 Additional results with deeper network

Table B.2: Parameters and settings used in the experiment.

| Network architecture | |
|-------------------------|---------------------|
| Name | Setting |
| Dimensions | [784, 100, 100, 10] |
| Activation function | ReLU |
| Random noise training | |
| Name | Setting |
| Number of examples | 5×10^5 |
| Batch size | 64 |
| Learning rate | 0.0001 |
| Optimizer | Adam |
| MNIST data training | |
| Name | Setting |
| Number of training data | 5×10^3 |
| Number of test data | 5×10^3 |
| Epochs | 100 |
| Batch size | 64 |
| Learning rate | 0.0001 |
| Optimizer | Adam |

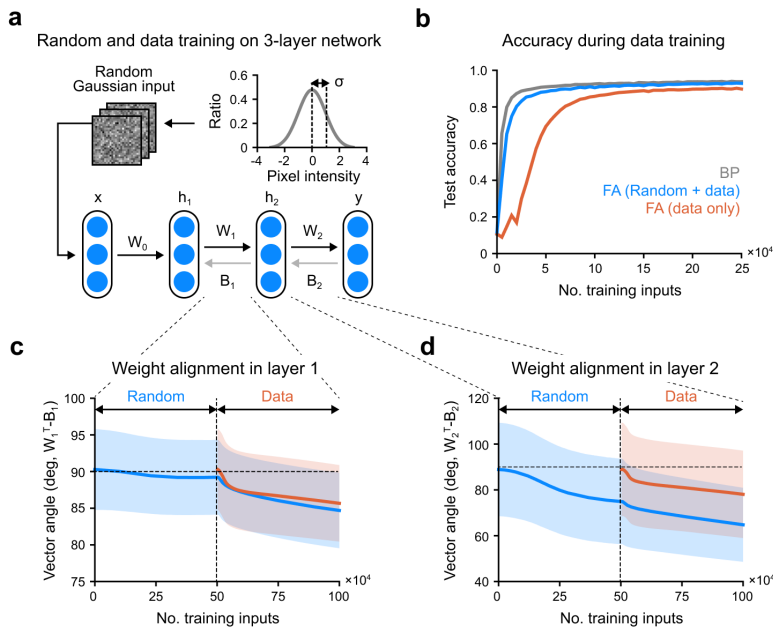


Figure B.3: Training with random noise and data in a deeper network. (a) Three-layer network trained with random noise and data sequentially. (b) Test accuracy of the network under various training conditions. (c) Alignment angle of the weights \mathbf{W}_1 and synaptic feedback \mathbf{B}_1 in the first layer of the network. (d) Alignment angle of the weights \mathbf{B}_2 and synaptic feedback \mathbf{W}_2 in the second layer of the network.

B.4 Additional results with CIFAR-10

Table B.3: Parameters and settings used in the experiment.

| Network architecture | |
|-------------------------|-----------------|
| Name | Setting |
| Dimensions | [3072, 100, 10] |
| Activation function | ReLU |
| Random noise training | |
| Name | Setting |
| Number of examples | 5×10^5 |
| Batch size | 64 |
| Learning rate | 0.0001 |
| Optimizer | Adam |
| CIFAR10 data training | |
| Name | Setting |
| Number of training data | 5×10^3 |
| Number of test data | 5×10^3 |
| Epochs | 100 |
| Batch size | 64 |
| Learning rate | 0.0001 |
| Optimizer | Adam |

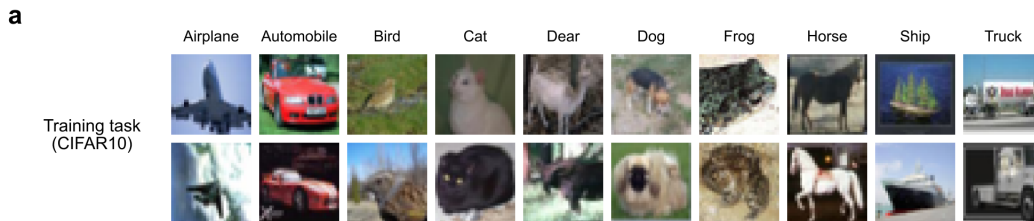


Figure B.4: Sample of the CIFAR-10 data [77] used in the subsequent data training process. The dataset contains images of ten classes, i.e. airplanes, cars, birds, cats, deer, dogs, frogs, horses, ships, and trucks.

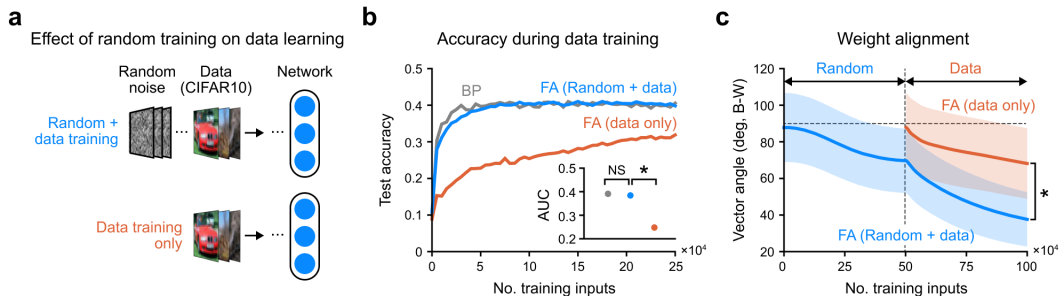


Figure B.5: Effect of random noise training on subsequent CIFAR-10 data training. (a) Design of the CIFAR-10 classification task. (b) Test accuracy during CIFAR-10 data training. (c) Alignment angle of weights \mathbf{W}_1 and synaptic feedback \mathbf{B}_1 during random noise training and subsequent CIFAR-10 data training.

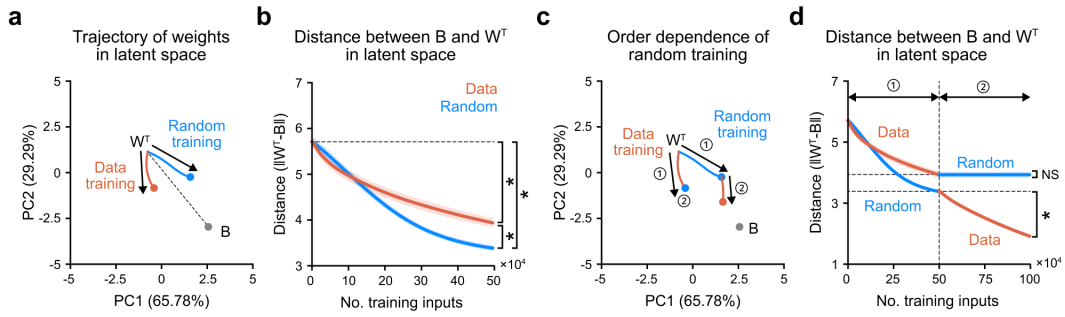


Figure B.6: Weight updates dynamic of random noise training and data training with CIFAR-10. (a) Trajectory of weights (W_1) toward synaptic feedback matrix (B_1) in the PCA (principal component analysis) latent space for random noise and CIFAR-10 data training. (b) Distance between weights (W_1) and the synaptic feedback matrix (B_1). (c) Order dependence of the trajectory of weights (W_1). (d) Distance between weights (W_1) and the synaptic feedback matrix (B_1) for alternating orders of random and CIFAR-10 data training.

C Experimental details and additional results for section 4.3

C.1 Network architecture and training details

Table C.1: Parameters and settings used in the experiment.

| Network architecture | |
|-----------------------|---------------------|
| Name | Setting |
| Dimensions | [784, 100, 100, 10] |
| Activation function | ReLU |
| Random noise training | |
| Name | Setting |
| Number of examples | 5×10^5 |
| Batch size | 64 |
| Learning rate | 0.0001 |
| Optimizer | Adam |

C.2 Refinement of readout probability by random noise training

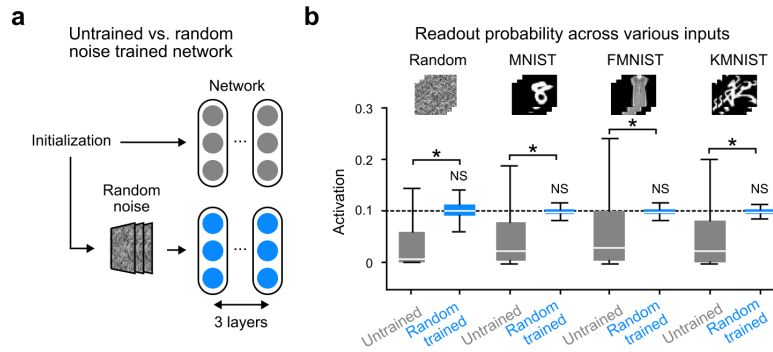


Figure C.1: Distribution of the readout probability. (a) Output probability of readout neurons measured in untrained and randomly trained networks. (b) Distribution of the readout probability of networks for various types of inputs: (1) Random noise, (2) MNIST data, (3) FMNIST data, and (4) KMNIST data.

C.3 Random noise training reduces the effective dimensionality of weights

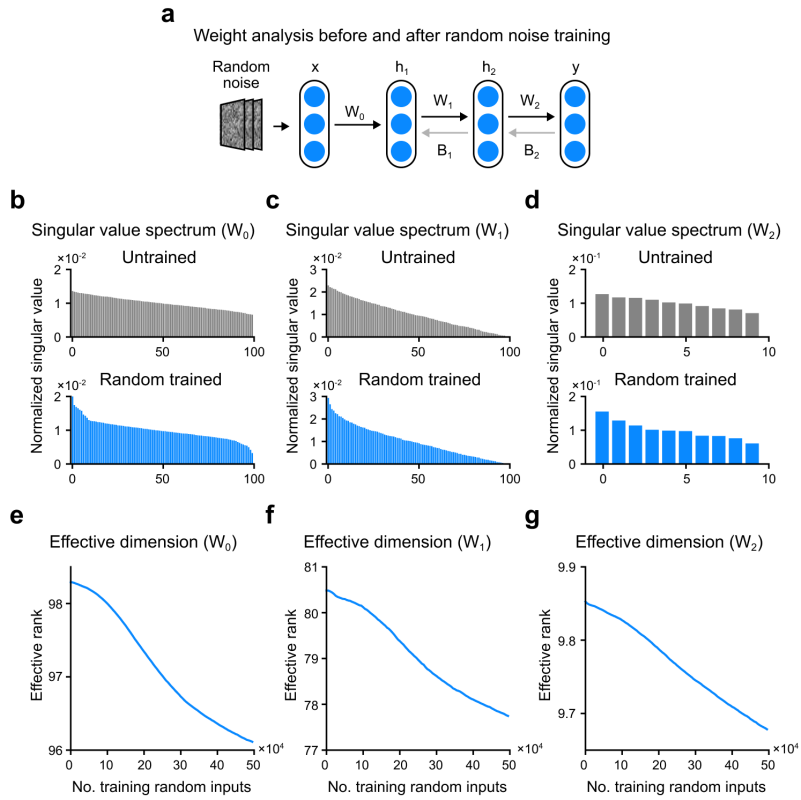


Figure C.2: Effective dimensionality of weights in various layers. (a) The architecture of the network used in the experiment in which the weights of the three layers are analyzed. (b-d) Singular value spectrum of weights in each layer of the untrained and randomly trained networks. (e-g) Effective dimensionality of weights in each layer during random noise training.

C.4 Training neural networks with various training sizes

Table C.2: Parameters and settings used in the experiment.

| Network architecture | |
|-------------------------|----------------------------|
| Name | Setting |
| Dimensions | [784, 100, 100, 10] |
| Activation function | ReLU |
| MNIST data training | |
| Name | Setting |
| Number of training data | [100, 200, 400, 800, 1600] |
| Number of test data | 1×10^3 |
| Epochs | 500 |
| Batch size | 64 |
| Learning rate | 0.0001 |
| Optimizer | Adam |

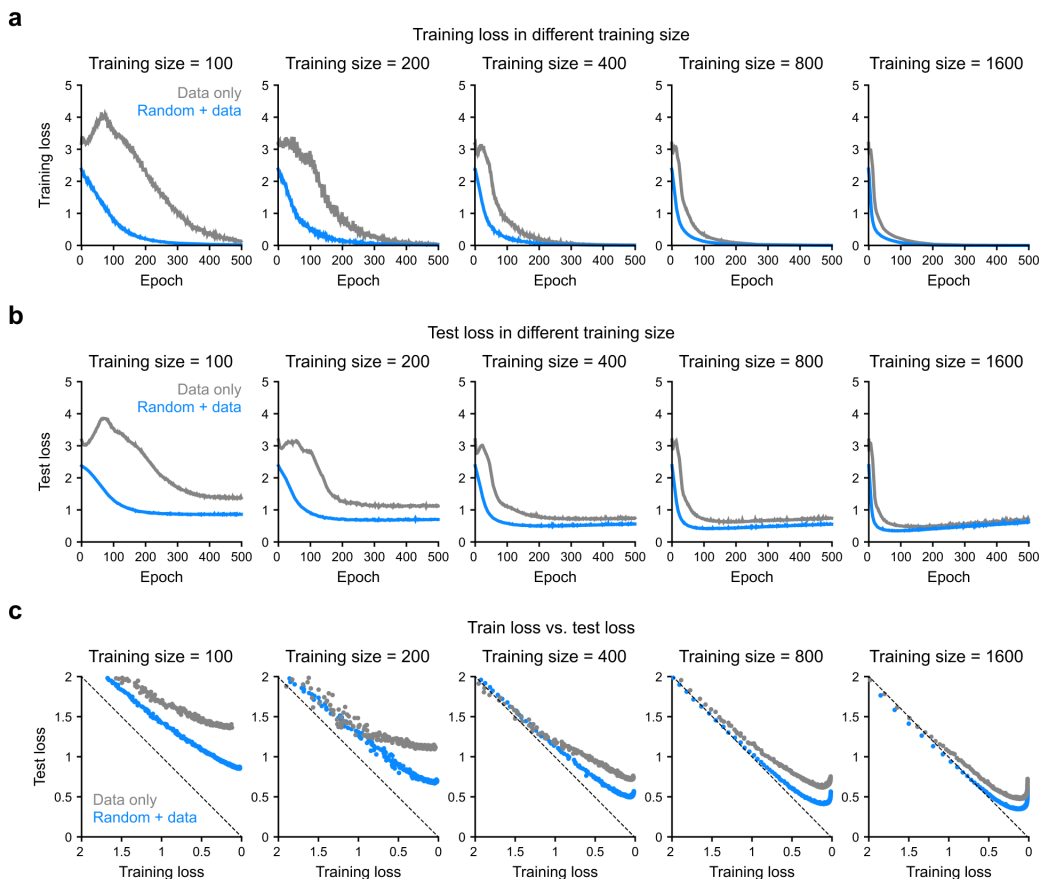


Figure C.3: Training process and generalization error for different training set sizes. (a) Training loss. (b) Test loss. (c) Training loss vs. test loss. Each column indicates a network trained with a different training set size, where gray and blue lines represent untrained and randomly pretrained networks, respectively.

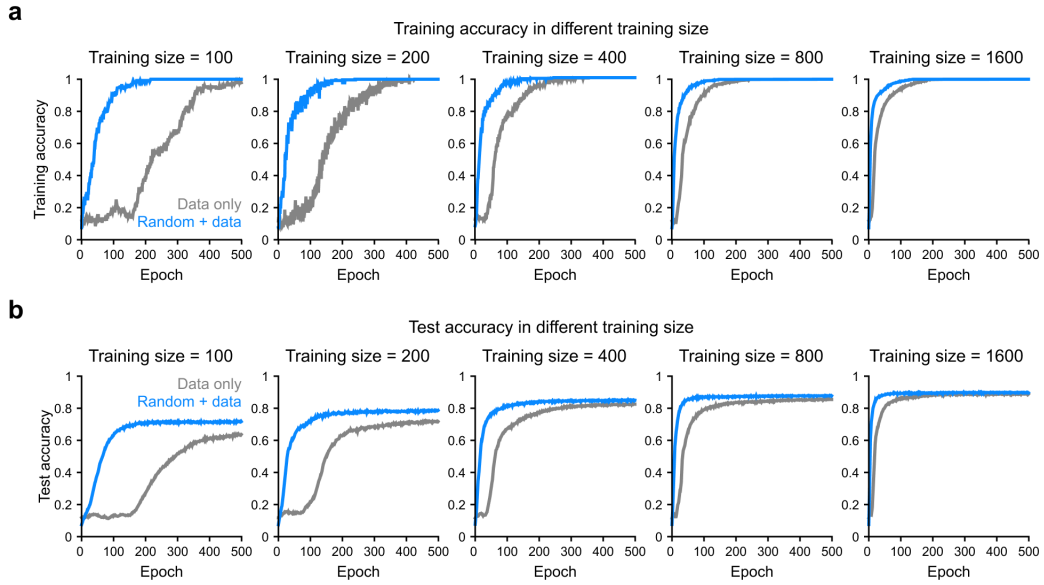


Figure C.4: Training and test accuracy for different training set sizes. (a) Training accuracy. (b) Test accuracy. Each column represents the network trained with different training set sizes. Gray and blue lines represent the untrained and randomly pretrained networks, respectively.

C.5 Training neural networks with various network depths

Table C.3: Parameters and settings used in the experiment.

| Network architecture | |
|----------------------------------------|-----------------|
| Name | Setting |
| Input, hidden layer, output dimensions | 784, 100, 10 |
| Number of hidden layers | [2, 3, 4, 5, 6] |
| Activation function | ReLU |
| MNIST data training | |
| Name | Setting |
| Number of training data | 1600 |
| Number of test data | 1×10^3 |
| Epochs | 500 |
| Batch size | 64 |
| Learning rate | 0.0001 |
| Optimizer | Adam |

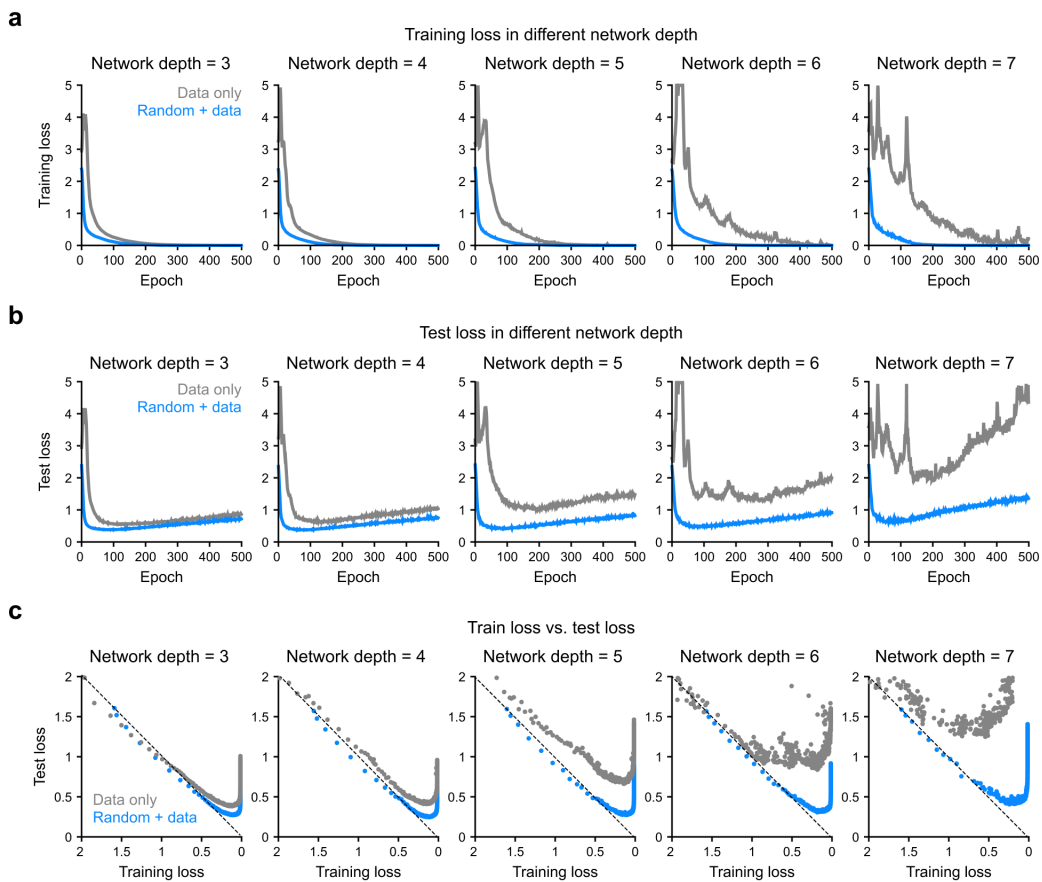


Figure C.5: Training process and generalization error for different network depths. (a) Training loss. (b) Test loss. (c) Training loss vs. test loss. Each column represents a network trained with a different network depth, where gray and blue lines represent untrained and randomly pretrained networks, respectively.

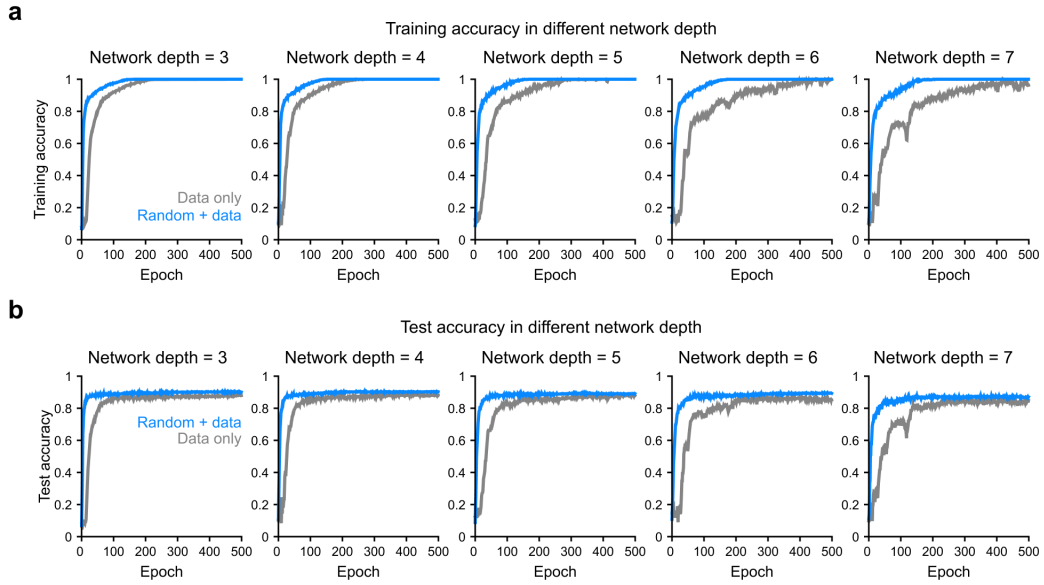


Figure C.6: Training and test accuracy with different network depths. (a) Training accuracy. (b) Test accuracy. Each column represents a network trained with a different network depth, where gray and blue lines represent untrained and randomly pretrained networks, respectively.

C.6 generalization test for out-of-distribution

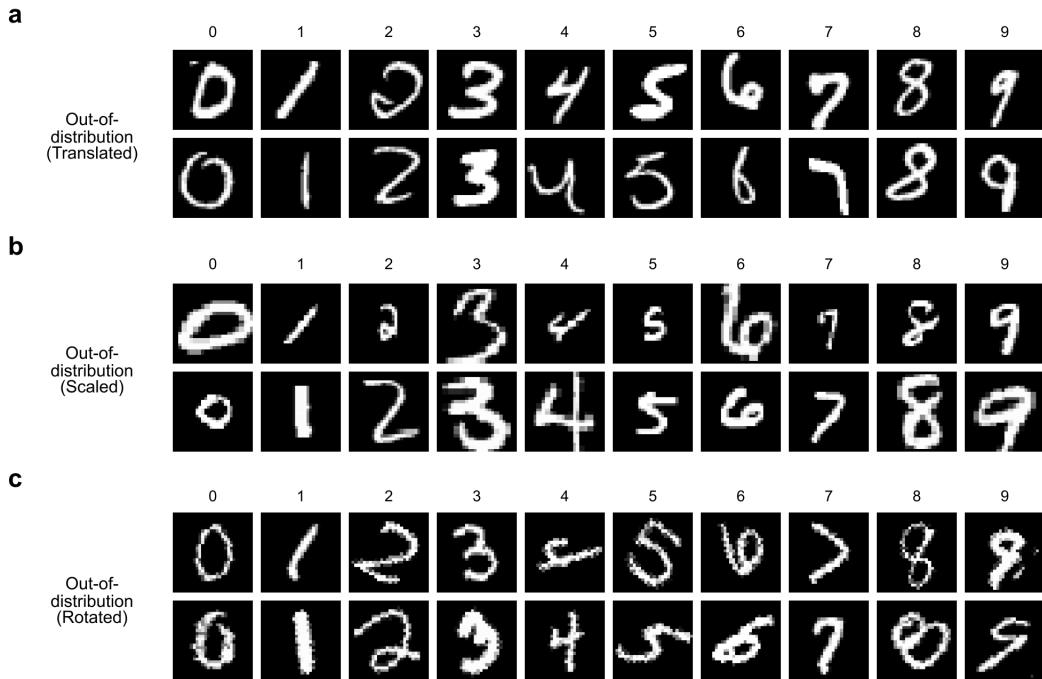


Figure C.7: Dataset used in the out-of-distribution generalization test with the transformed dataset. (a) MNIST dataset used in the training in-distribution case. (b-d) Transformed MNIST dataset used in the generalization test in the out-of-distribution case. (b) Translated MNIST dataset, where each image is randomly translated in the range of $[-5\%, 5\%]$ of the input image size on the x- and y-axis. (c) Scaled MNIST dataset. Each image is randomly scaled in the range of $[0.8, 1.2]$. (d) Rotated MNIST dataset. Each image is randomly rotated in the range of $[-25, 25]$ degrees.

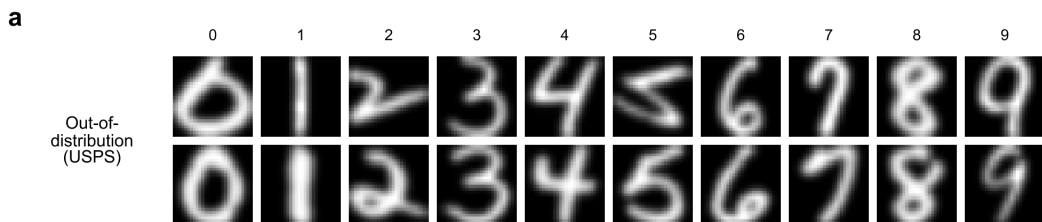


Figure C.8: Dataset used in the out-of-distribution generalization test with benchmark dataset. (a) MNIST dataset [52] used in the training the networks in the out-of-distribution case. (b) USPS dataset [78] resized from (16×16) to (28×28) used in the generalization test in the out-of-distribution case.

D Experimental details and additional results for section 4.4

D.1 Network architecture and training details

Table D.1: Parameters and settings used in the experiment.

| Network architecture | |
|-------------------------|---------------------|
| Name | Setting |
| Dimensions | [784, 100, 100, 10] |
| Activation function | ReLU |
| Random noise training | |
| Name | Setting |
| Number of examples | 5×10^5 |
| Batch size | 64 |
| Learning rate | 0.0001 |
| Optimizer | Adam |
| Meta-loss measurement | |
| Name | Setting |
| K | 10 |
| Inner steps | 10 |
| Inner learning rate | 0.001 |
| Optimizer | Adam |
| Various task adaption | |
| Name | Setting |
| Number of training data | 5×10^3 |
| Number of test data | 5×10^3 |
| Epochs | 100 |
| Batch size | 64 |
| Learning rate | 0.0001 |
| Optimizer | Adam |

D.2 Tasks used during the measurement of meta-loss

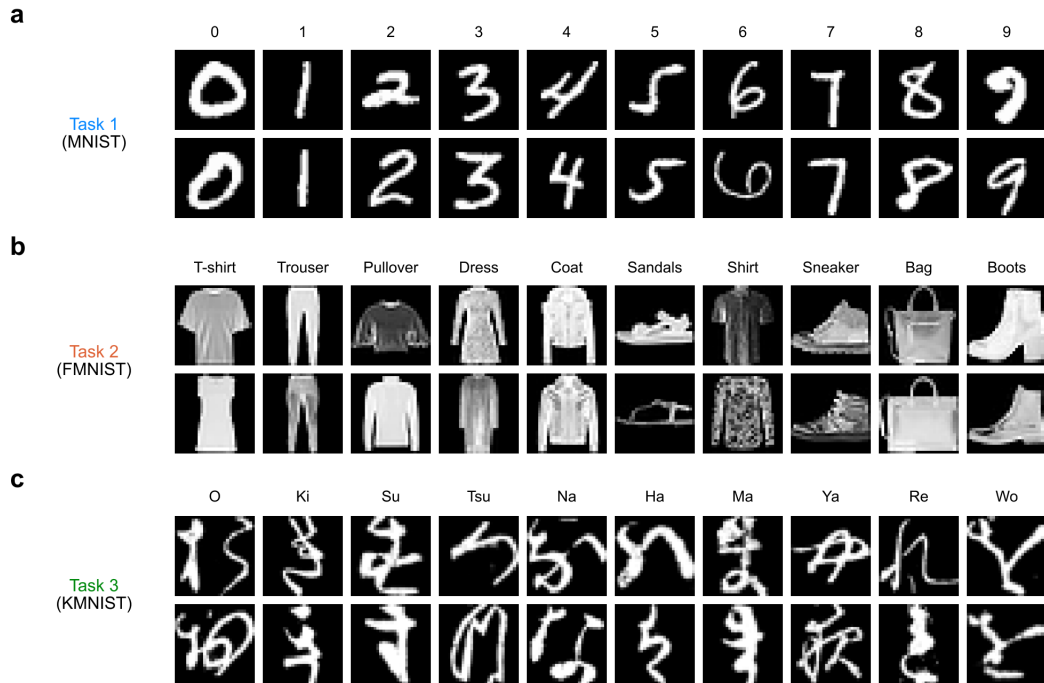


Figure D.1: Tasks used to measure the meta-loss. (a) Task 1: MNIST [52] classification task. (b) Task 2: Fashion-MNIST [55] classification task. (c) Task 3: Kuzushiji-MNIST [56] classification task.

E Experimental environment

E.1 Data availability

The datasets used in this study are publicly available. The MNIST dataset is available at <http://yann.lecun.com/exdb/mnist/>. The USPS dataset is available at <https://www.csie.ntu.edu.tw/~cjlin/libsvmtools/datasets/multiclass.html#usps>. The Fashion-MNIST dataset is available at <https://github.com/zalandoresearch/fashion-mnist>. The Kuzushiji-MNIST dataset is available at <https://github.com/rois-codh/kmnist>. The CIFAR-10 dataset is available at <https://www.cs.toronto.edu/~kriz/cifar.html>.

E.2 Software used

Python 3.11 (Python software foundation) with PyTorch 2.1 and NumPy 1.26.0 was used to perform the simulation and the analysis. SciPy 1.11.4 was used to perform the statistical test and analysis. The custom Python codes used in this work will be made available at the GitHub repository after the publication of the paper.

E.3 Computing resources

All simulations were performed on a computer with an Intel Core i7-11700K CPU and an NVIDIA GeForce RTX 1080 GPU. The simulation code was parallelized using PyTorch's built-in parallelization to utilize the GPU resources efficiently.